Supporting Information

Bouvet et al. 10.1073/pnas.1201130109

SI Text

Biochemical Characterization of Severe Acute Respiratory Syndrome Coronavirus nsp14 Exoribonuclease Activity in the Presence of nsp10 Activating Factor. For insight into the nonstructural protein 14 (nsp14) 3′–5′ exoribonuclease (ExoN) activity in the presence of nsp10 stimulating factor, we further analyzed the condition for optimal RNA hydrolytic activity. For this purpose, we performed ExoN assay using *p-H4 RNA substrate in various experimental conditions, and the ExoN activity was quantified. As shown in Fig. S1*A*, nsp10/nsp14 exhibits maximal hydrolytic activity peaking between pH 7.0 and 8.5. As shown in Fig. S1*B*, reducing agents such as DTT may stabilize the nsp14 protein and enhance its ExoN activity. In contrast, the addition of increasing NaCl concentrations limits the ExoN activity of nsp14 (Fig. S1*C*). The ExoN activity of nsp14 was next analyzed according to the optimal conditions determined in 40 mM Tris·HCl (pH 8) and 5 mM DTT in the presence of fourfold molar excess of nsp10 protein over nsp14 (200 nM/50 nM when no contrary indications).

Nsp10/nsp14 ExoN Requires Functional Zn^{2+} Fingers in nsp10 and Catalytic Mg^{2+} in nsp14. Nsp14 ExoN belongs to the ExoN [exo (ribo)nucleases] containing a conserved Asp-Glu-Asp-Asp motif (DEDD) nuclease superfamily (DEDDh subfamily) whose members critically depend on divalent cations to exert their catalytic activity. Nsp10 carries a zinc-finger domain required for correct folding (1, 2). As shown in Fig. 2*B*, we observe nsp10/nsp14 ExoN activity in the absence of exogenous metallic cations, suggesting that metallic ions might have copurified and remained associated with the proteins. Incubating the proteins with 0.5 mM EDTA prior to addition of *p-H4 RNA substrate inhibits ExoN activity, but the latter can be restored and even slightly stimulated by the subsequent addition of 1.5 mM $MgCl_2$. The addition of 1.5 mM $MnCl_2$ leads to the recovery of a weak ExoN activity. The addition of 3 mM of $MgCl_2$ or $MnCl_2$ also reactivates the ExoN activity, albeit to a lesser extent, indicating that high ion concentrations have an inhibitory effect on nsp10/nsp14 activity. These results confirm that nsp10/nsp14 ExoN activity depends on metallic ions, preferentially magnesium over manganese. Moreover, our results also suggest that the nsp10 Zn^{2+} structural ions are not removed by the 0.5-mM EDTA treatment.

To further investigate the importance of the nsp10 zinc-finger structural integrity in the activation of nsp14 ExoN, we removed the zinc ions bound to nsp10 using 10 mM EDTA and subsequently eliminated the chelating agent by dialysis. As shown in Fig. 2*C*, the pretreatment of nsp10 with EDTA blocks its stimulatory effect on nsp14 ExoN activity. The supplementation of the reaction mix with 2 mM $MgCl_2$ does not restore the hydrolytic activity, indicating that Mg^{2+} does not substitute for Zn^{2+} in the nsp10 zinc finger. In contrast, the addition of 20 μM $ZnCl_2$ in the reaction mix leads to the recovery of nsp10/nsp14 ExoN activity. Together, these results demonstrate that Mg^{2+} is required for nsp14 ExoN activity and that the nsp10 zinc fingers must be loaded with zinc ions to stimulate nsp14 ExoN.

Nsp10/nsp14 ExoN Requires a Base-Paired 3′-End on the RNA Substrate. A set of 5′-end radiolabeled RNAs was used to address substrate requirements of the nsp10/nsp14 ExoN activity. Fig. S4 shows, as controls, that nsp14 alone does not exhibit significant nuclease activity under the conditions used here, whereas in presence of nsp10, the *p-H4 RNA is hydrolyzed in a time-dependent manner. Concerning other substrates, *p-H1 and *p-LE19 RNAs are efficiently degraded in presence of nsp10/nsp14, leading to the removal of ∼2 and 5 nt from the substrate RNA, respectively. *p-RNA3 is hydrolyzed in a lesser extent, and *p-RNA6 is slightly shortened into laddering products. Other substrates (*p-RNA11, *p-O4, *p-O9, *p-C15, and *p-A30) resisted nsp10/nsp14-mediated degradation.

We predicted the secondary structures adopted by the different RNAs using Mfold RNA modeling server (http://mfold.rna.albany.edu/?q=mfold; Fig. S3). The comparison of the predicted structures to the cleavage efficiency mediated by nsp10/nsp14 ExoN toward the substrates shows that RNAs predicted to adopt a stable hairpin structure at their 3′-end (like H1 or H4) are efficiently hydrolyzed by nsp10/nsp14. RNAs forming unstable structures and/or having few protruding 3′ nucleotides (like RNA6 or RNA3 respectively) resist nsp14 cleavage. Last, RNAs presenting long, free 3′-ends, after a stem-loop structure, weak hairpin structures, or being entirely 3′ single-stranded (like RNA11, O9 and O4, and C15 and A30) are barely hydrolyzed by nsp10/nsp14 ExoN. LE19 RNA is predicted to be linear in solution but can hybridize to form a duplex with a ΔG of −4.50 kcal/mol, thus exhibiting a 3′-end whose ultimate bases are paired; it is accordingly degraded by the nsp10/nsp14 complex.

We conclude that a base-paired 3′-end is a prerequisite of nsp10/nsp14 ExoN activity. Moreover, the stability of the structure is important because structures predicted to exhibit the lower ΔG are the most efficiently hydrolyzed, which may explain why few nucleotides are hydrolyzed after initial 3′ degradation. Indeed, 3′ structures are destabilized, leading to a linear form of the digested RNA becoming nonsusceptible to nsp10/nsp14 degradation.

1. Pan J, et al. (2008) Genome-wide analysis of protein-protein interactions and involvement of viral proteins in SARS-CoV replication. *PLoS ONE* 3:e3299.

2. Joseph JS, et al. (2006) Crystal structure of nonstructural protein 10 from the severe acute respiratory syndrome coronavirus reveals a novel fold with two zinc-binding motifs. *J Virol* 80:7894–7901.

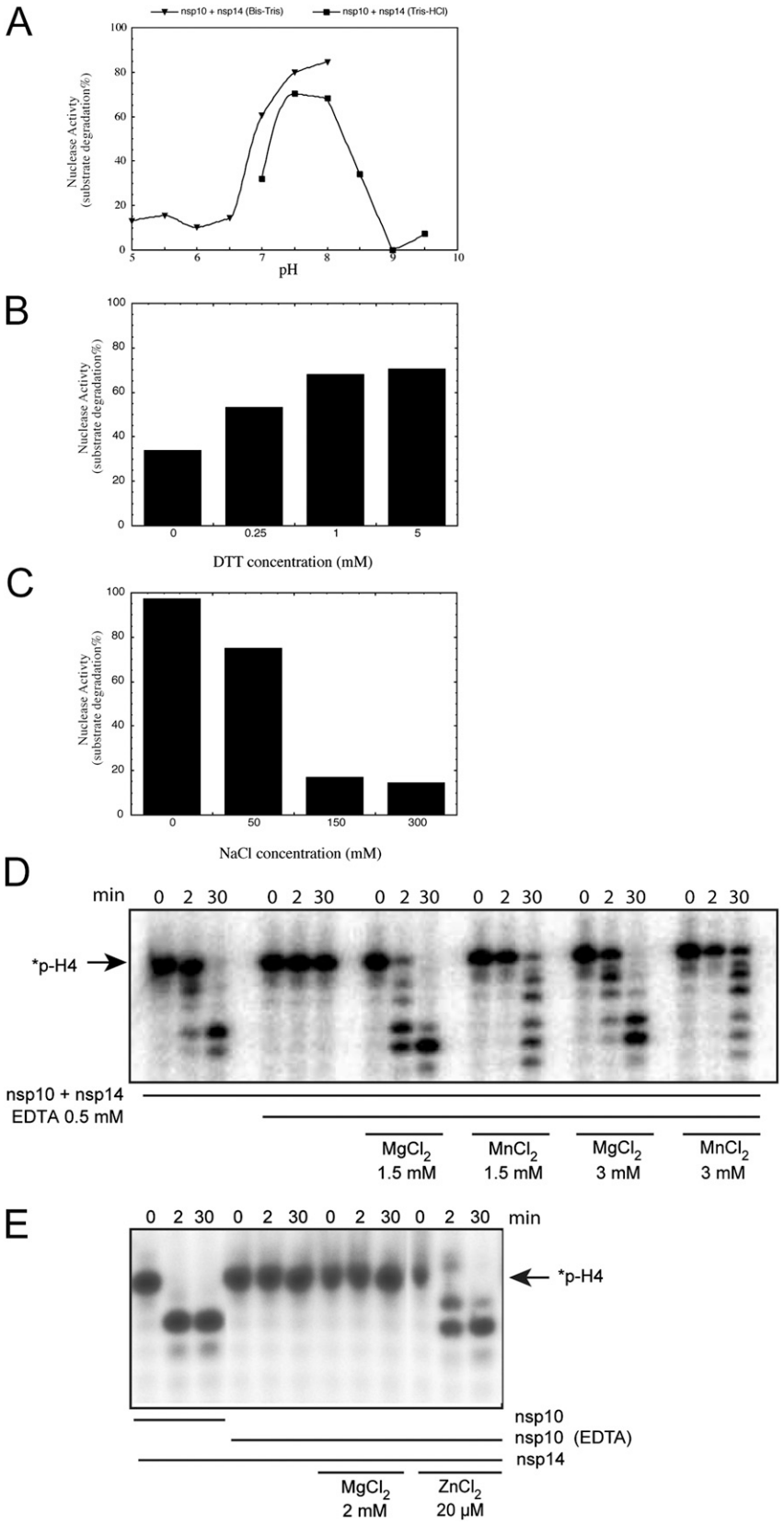

Fig. S1. Biochemical characterization and ion requirements of the nsp10/nsp14 ExoN activity. ExoN activity was followed by incubating *p-H4 RNA with nsp14 in the presence of nsp10 during 5 min. Digestion products were analyzed by denaturing Urea-PAGE and revealed by autoradiography. The ExoN activity was measured by quantifying disappearance of the *p-H4 band using a PhosphorImager and Image Gauge software. Standard conditions are as follows: 40 mM Tris·HCl (pH 8), 5 mM DTT, 50 nM nsp14, and 200 nM nsp10 in the presence of 750 nM of ^{32}P-labeled *p-H4 RNA oligonucleotide (*SI Text*). (*A*) The pH dependence of the nsp10/nsp14 ExoN activity was determined in buffers of increasing pH, from pH 5 to 8 in 50 mM Bis-Tris and from pH 7 to 9.5 in Tris·HCl buffer.

Legend continued on following page

(*B* and *C*) Effect of increasing concentrations of DTT and NaCl on the nsp10/nsp14 ExoN activity, respectively. (*D*) Cation-dependent cleavage assays. *p-H4 RNA was incubated with nsp10/nsp14 proteins during 0, 2, and 30 min in the presence of EDTA (0.5 mM) and supplemented or not with $MgCl_2$ or $MnCl_2$ (1.5 mM and 3 mM). Reaction products were then separated on a 20% (wt/vol) denaturing Urea-PAGE, and digestion products were revealed by autoradiography. Composition of the reaction mixture is indicated at the bottom of the panel. (*E*) Cation-dependent nsp10-mediated stimulation assay. *p-H4 RNA was incubated with nsp14 and nsp10 preincubated or not with 10 mM EDTA in the absence or presence of exogenous $MgCl_2$ (2 mM) or $ZnCl_2$ (20 μM). Reaction products were then separated on a 20% (wt/vol) denaturing Urea-PAGE and revealed by autoradiography. The composition of the reaction mixture is indicated at the bottom of the panel.

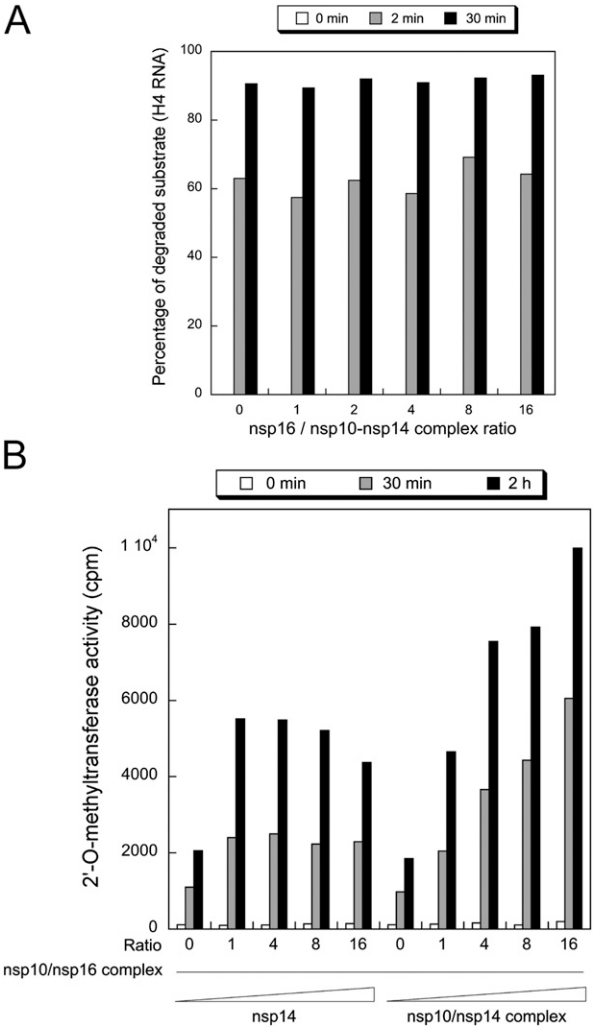

Fig. S2. Competition experiments. (*A*) A constant concentration (5 nM) of purified nsp10/nsp14 complex in the absence or presence of various concentrations of nsp16 protein (at molecular excess ratio of 0, 1, 2, 4, 8, and 16) was incubated with radiolabeled H4 RNA substrate. Reactions were stopped at 0, 2, and 30 min, and reaction products were separated using denaturing Urea-PAGE. Degradation of the H4 RNA substrate was quantified using PhosphorImager and Image Gauge software. (*B*) A constant concentration (200 nM) of purified nsp10/nsp16 complex in the presence of various concentrations of either nsp14- or nsp10/nsp14-purified complex proteins (at molecular excess ratio of 0, 1, 4, 8, and 16) was incubated with an 8-mer RNA corresponding to the 5′ extremity of the severe acute respiratory syndrome coronavirus genome carrying a N7-methylated cap structure and radiolabeled *S*-adenosyl-L-methionine. Reactions were stopped at 0, 30 min, and 2 h, and reaction products were collected on a diethylaminoethyl (DEAE) filter. Filters were washed, and the radiolabel transferred to RNA was counted to measure 2′-O-methyltransferase activity.

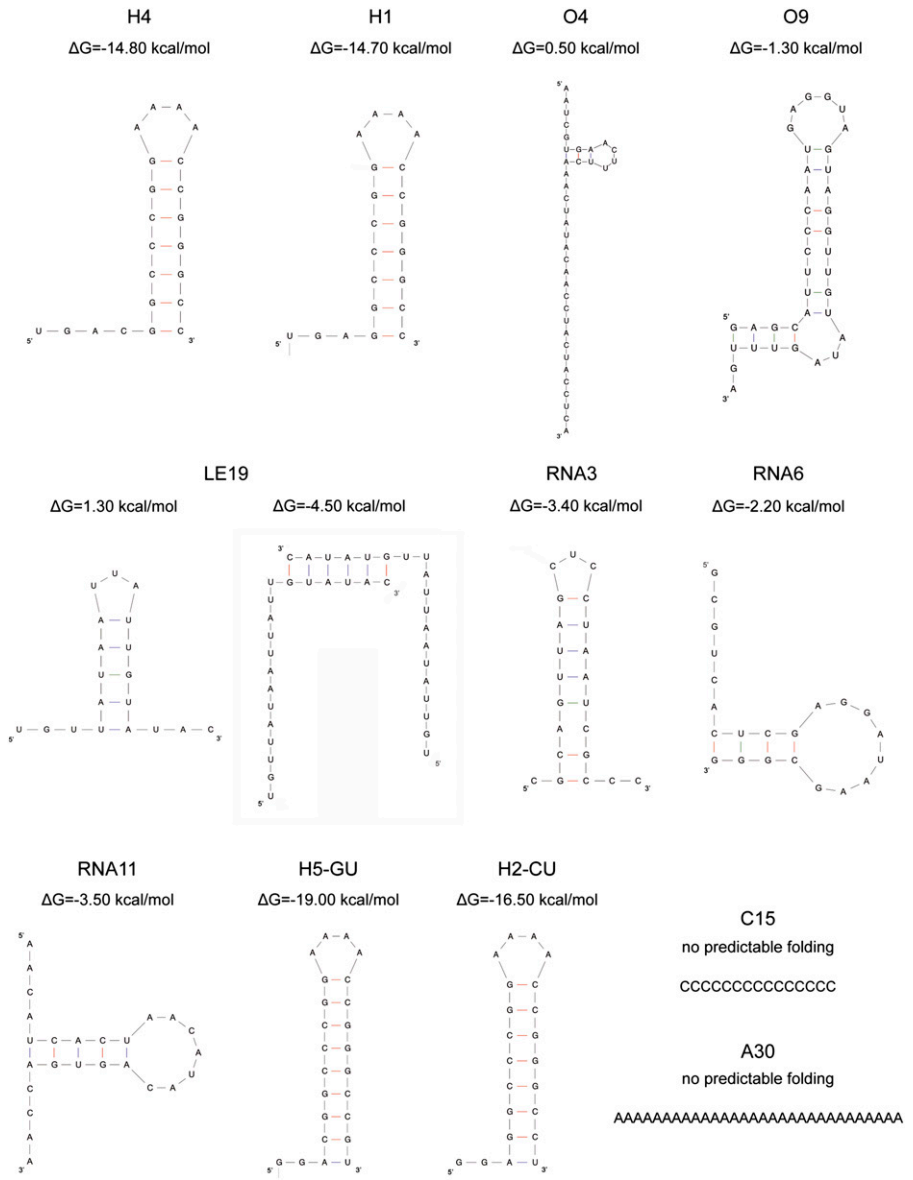

Fig. S3. Predicted structures adopted by substrate RNAs used in this study. The sequences of the different RNAs used in this study are presented in Table S1, and their most stable predicted structure obtained using Mfold RNA modeling server (http://mfold.rna.albany.edu/?q=mfold) is shown, as well as the minimum free energy (ΔG).

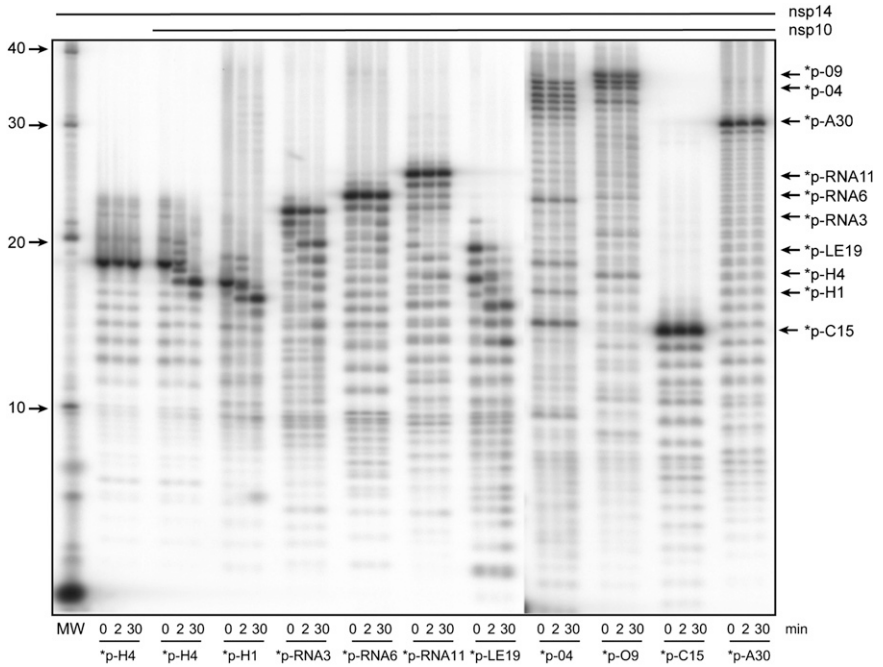

Fig. S4. Determination of nsp10/nsp14 ExoN substrate requirements. HPLC -purified ssRNAs of various lengths and structures were labeled at their 5′-end using polynucleotide kinase (PNK) in the presence of [γ^{32}P]ATP. RNAs were then incubated (0, 2, and 30 min) with purified nsp10 and nsp14. Reaction products were separated on a 20% (wt/vol) denaturing Urea-PAGE and revealed by autoradiography. ^{32}P-labeled molecular weight marker sizes are indicated on the left of the panel. Sequences and predicted structures of RNAs, as well as the minimum free energy (ΔG) of each RNA, calculated using Mfold, are presented in Table S1 and Fig. S3.

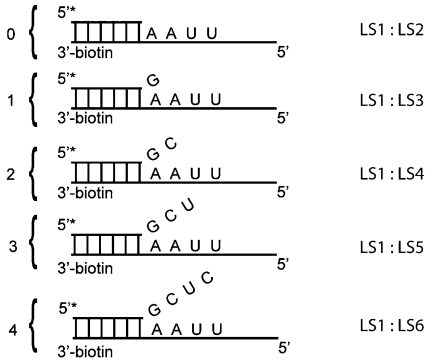

Fig. S5. Schematic representation of the substrates mimicking replication intermediates. LS1 RNA carrying a biotin group at its 3′extremity was annealed with LS2, LS3, LS4, LS5, and LS6 RNAs to generate duplex RNAs mimicking a replication intermediate with incorporation of 0, 1, 2, 3, or 4 mismatched nucleotides, respectively.

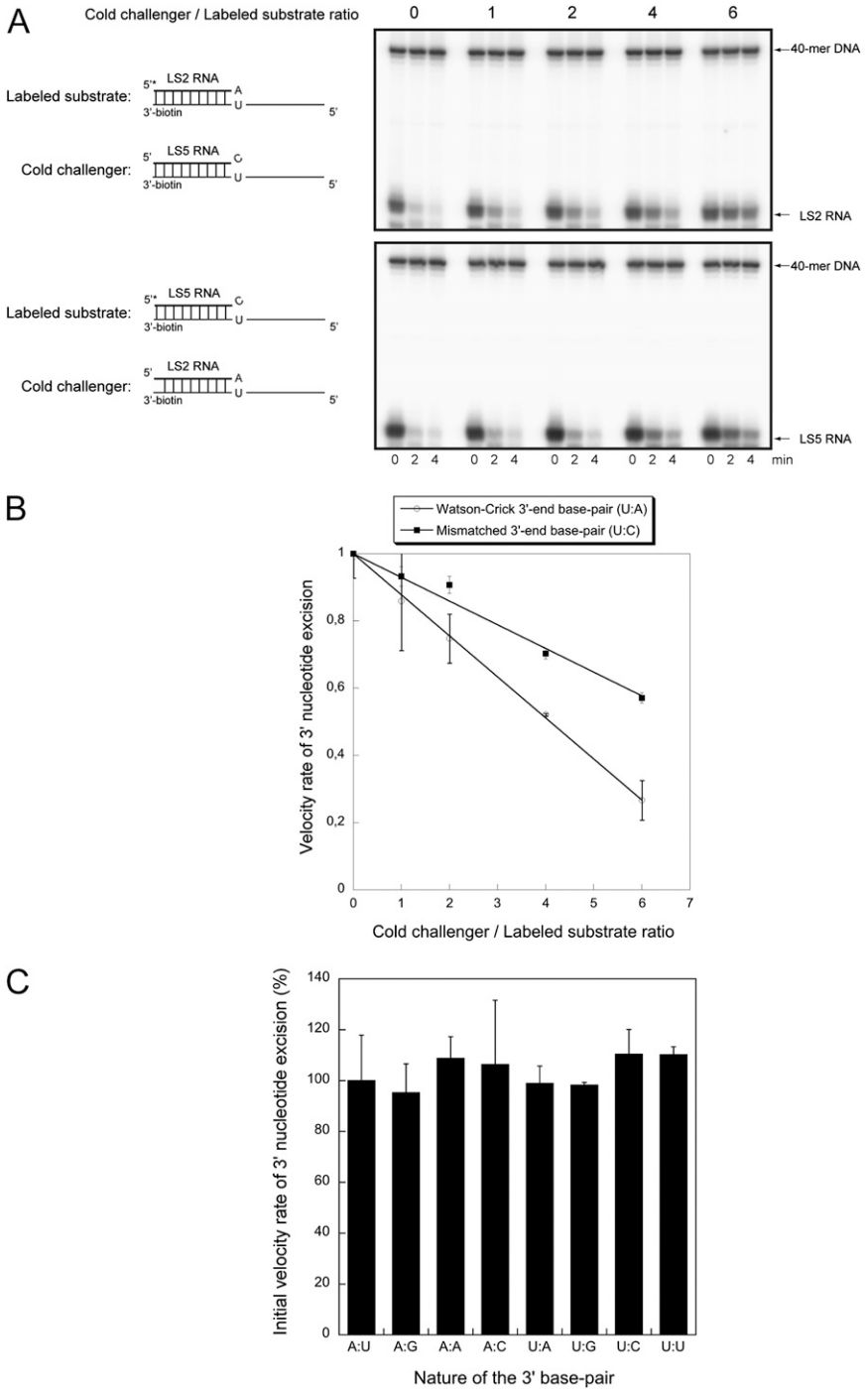

Fig. S6. Nsp10/nsp14 ExoN activity on various mismatches. (*A*) A 40-mer RNA (LS1) biotinylated in 3′ was annealed with a 5′-radiolabeled oligoribonucleotide resulting in either a Watson–Crick (U:A) or a mismatched (U:C) 3′-end base pair, as depicted on the left side of the panel. These duplexes were then incubated 0, 2, and 4 min with purified nsp10 and nsp14 in the absence or presence of cold challenger RNA. Cold substrate carrying a mismatched 3′-end base pair was used to compete the degradation of the radiolabeled substrate carrying a Watson–Crick 3′-end base pair (*Upper*) and inversely (*Lower*). Cold challenger was used at increasing concentrations giving a zero, one-, two-, four-, and sixfold molar ratio over radiolabeled substrate. Reaction products were separated on a 20% (wt/vol) denaturing Urea-PAGE and revealed by autoradiography. (*B*) Using data of *A*, the 3′ nucleotide excision rate was calculated and plotted as a function of cold challenger/labeled substrate ratio. (*C*) A 3′ biotinylated 40-mer RNA (LS1) was annealed with a 5′-radiolabeled oligoribonucleotide carrying 0 or 1 noncomplementary base at its 3′-end, as depicted in Fig. S5. Duplex RNAs carrying different mismatched 3′ base pairs (indicated at the bottom of the bar graph) were then incubated 0, 2, 4, and 6 min with purified nsp10/nsp14. Reaction products were separated on a 20% (wt/vol) denaturing Urea-PAGE and revealed by autoradiography. A radiolabeled 40-mer DNA was introduced in the reaction mixture as an internal quantification reference. Kinetics of mismatched nucleotides excision was compared with that of paired nucleotides (A:U = 100%).

Table S1. RNA sequences

RNA name	5′–3′ sequence
H4	UGACGGCCCGGAAAACCGGGCC
H1	UGAGGCCCGGAAAACCGGGCC
O4	AAUCGUGAACUUUCAAACUAUACAACCUACUACCUCA
O9	GAGCAUUCCCAAUGAGGUAGUAGGUUGUAUAGUUUGA
LE19	UGUUAUAAUUAUUGUAUAC
RNA3	CGCAGUUAGCUCCUAAUCGCCC
RNA6	GCGUCACUCGAGGAUAAGCGGG
RNA11	AACAUCACUAACAUACAGUGACCAA
C15	CCCCCCCCCCCCCCC
A30	AAAAAAAAAAAAAAAAAAAAAAAAAAAAAA
H5-GU	GGACGGCCCGGAAAACCGGGCCGU
H2-CU	GGAGGCCCGGAAAACCGGGCCU
RNA11revbiot	UUGGUCACUGUAUGUUAGUGAUGUU
H2-CUU(N)10	GGAGGCCCGGAAAACCGGGCCUUCACACACACA
H5-GUU(N)10	GGACGGCCCGGAAAACCGGGCCGUUAUGUCAUGAC
LS1	CUAUCCCCAUGUGAUUUUAAUAGCUUCUUAGGAGAAUGAC
LS2	GUCAUUCUCCUAAGAAGCUA
LS3	GUCAUUCUCCUAAGAAGCUAG
LS4	GUCAUUCUCCUAAGAAGCUAGC
LS5	GUCAUUCUCCUAAGAAGCUAGCU
LS6	GUCAUUCUCCUAAGAAGCUAGCUC

Sequences of RNA substrates used in this study are listed with their corresponding name. Sequences are presented from 5′ to 3′.